Lattice Mesoscale modelling of Chloride Penetration in Concrete: Effect of aggregate volume fraction and fly ash

Truong Son Bui[1], Duc Tho Pham[1*], Minh Ngoc Vu[2], Van Duc Bui[1], Nam Hung Tran[3], and Thi Nu Nguyen[1]

[1] *Hanoi University of Mining and Geology, Hanoi, Viet Nam*
[2] *Duy Tan University, Da Nang, Viet Nam*
[3] *Le Quy Don Technical University, Hanoi, Viet Nam*
[*] *Corresponding author. E-mail: phamductho@humg.edu.vn*

Chloride ions penetrated into reinforced concrete member causes rebar corrosion and induces the volume expansion of the rebar and cracks of concrete cover. This study aims to predict the chloride ingress in the reinforced concrete member and its operational service life by using a lattice model. Concrete is considered at the mesoscale, which constitutes three phases: aggregates, cement matrix and interfacial transition zones (ITZ). Fick's second law was implemented into the lattice model to describe the diffusion of the chloride ions within concrete. The diffusivity coefficient of aggregates is almost null, whereas those of cement paste and of ITZ are deduced from macroscopic diffusivity measure. Numerical solutions is validated against the test data and the analytical solution. The effect of the aggregate volume fraction is discussed. Curves, which help to determine the service life of the reinforced concrete structure from the cover thickness, is resulted from the lattice modelling for concrete with different aggregate volume fractions.

1. Introduction

Chloride penetration induced corrosion of steel reinforcement is one of the major degradation mechanisms of reinforced concrete (RC) structures under coastal and marine conditions. The chloride diffusivity coefficient defines the capacity of a concrete to resist chloride penetration. Several methodologies have been developed to measure this coefficient [1–5]. Besides, micromechanical approach is an alternative method to estimate the macroscopic diffusion property of concrete when the diffusivity is known for the aggregate and the cement matrix [6–8]. Once, the macroscopic coefficient is available, the diffusion of chloride ions in concrete is usually described by Fick's second law where the macroscopic diffusivity is an input parameter. Analytical solutions are only available for some simple configurations such as 1D or axisymmetric diffusion problems. Therefore, numerical modelling is widely applied for predicting chloride concentration in concrete structures.

Macroscopic modelling, based on finite element method Pouya [9], boundary element method [10, 11], meshless methods [12] is inappropriate to provide the local information. Thus, concrete is usually considered at a mesoscale with three phases: aggregates, cement paste and ITZ for a better understanding the local behaviour, as well as the interaction between different components and reinforced bars. A mesoscopic classical FEM model with a softening constitutive model could lead to the mesh sensitive results [13, 14]. The FEM with the introduction of zero-thickness interfaces in the mesh, so-called discrete crack approach [15, 16] is an alternative approach, which needs a very

fine to reduce the mesh dependent result. This limitation in mesh-dependent result can be overcome by using the lattice modeling, which has been shown to be mesh-independent when modeling the mechanical behavior of concrete with the softening and residual features [17].

Moreover, lattice models are particularly interesting in heterogeneous cement composites, since they allow considering the effects on the overall damage law of microcracking [18–23], aggregate and pores [21], as well as their statistical interaction [24]. However, the Fick's second law for modeling the chloride diffusion have not existed in the lattice code yet. This work presents the implementation of Fick's second law into the lattice model to describe the chloride diffusion within concrete at the mesoscale. This mesoscopic lattice model considers that concrete is constituted by three phrases aggregate, cement and ITZ. Input parameters of the proposed model are the diffusivity coefficient of these three concrete constitutions. They are determined from test data measured on the concrete of grade G40 sample, a representative ordinary concrete commonly used as the main bearing structures in construction and building.

Comparison with analytical solution and experiment result is made to show the validation of the proposed model. The influences of the aggregate volume fraction and of fly ash on the macroscopic diffusivity are evaluated. Curves describing the relation "cover thickness - life service" is proposed for the concrete G40 with different aggregate volume fractions, as well as with or without fly ash. These curves are the result of the lattice simulation. A closed-form solution is also developed to assess the concrete cover thickness corresponding to a considered environment condition and a chloride concentration threshold with respect to the rebar corrosion. This analytical solution is in a good agreement with the numerical one obtained for G40 concrete. The latter result can be applied for different concrete grades and for every environment chloride concentration condition. Therefore, this is really useful for aided design of RC structure subjected to aggressive environment.

2. Numerical modelling

2.1. Lattice Model

The lattice model for modelling the heat and mass transfer is developed based on the Voronoi tessellation of the domain [25]. The coupling between two physics: mechanic and transport (mass or heat transfer) is done by adding the Delaunay triangulation, where the mechanical elements are placed along the edges of the Delaunay triangles, while conduit elements are along the edges of the Voronoi polygons. Lattice models connect nodes, which are the nuclei of the

neighboring Voronoi polygons. The nodes are randomly generated in the domain (S_d), constrained by two parameters: the minimum allowable distance, d_{min}, between nodes and the spatial density of nodes (ρ_n). The node density determines the distribution of distances between nodes by the following relation

$$\rho_n = \frac{N_n d_{\min}^2}{S_d} \tag{1}$$

in which N_n is the number of nodes. d_{min} and (ρ_n) should be large enough to avoid the numerical divergence.

The material response of the transport elements is calculated, as for the structural elements, at point C (Fig. 1(b)).

Fick's second law is implemented within Lattice model to simulate the diffusion of chloride ions within the concrete structure. The discrete form of the differential equation for a one-dimensional transport element is:

$$D_e C + C_e \frac{\partial C}{\partial t} = f \tag{2}$$

where D_e is the diffusion coefficient matrix, C_e the capacity matrix, t the time and f the nodal flow rate vector. The diffusion matrix and the capacity matrix are defined as

$$D_e = \frac{h}{l} D_t \begin{pmatrix} 1 & -1 \\ -1 & 1 \end{pmatrix}; \quad C_e = \frac{hl}{12} \begin{pmatrix} 2 & 1 \\ 1 & 2 \end{pmatrix} \tag{3}$$

2.2. Model Validation

For 1D transport within a bar with length L and with the following initial and boundary condition (Fig. 2).

$$C(x = 0, t) = C(x = L, t) = 0$$
$$\text{and } C(x, 0) = \sin\left(\frac{\pi x}{L}\right) \tag{4}$$

The diffusivity coefficient is assumed to be unity, the explicit solution of Equation (1) is well known as follows [26]:

$$C(x, t) = \sin\left(\frac{\pi x}{L}\right) e^{\frac{-\pi^2 t}{L^2}} \tag{5}$$

Fig. 3 shows the comparison results between solutions of the chloride diffusion obtained from equation (5) and the proposed lattice model. A perfect agreement between the present model and the closed-form solution is observed.

2.3. Geometry and boundary condition

A 2D rectangular specimen of 100x200 (mm) is considered that respects the minimum length side (100 mm) of a 2D representative volume element (RVE) for concrete material [18, 27, 28] (Fig. 4). The aggregate diameter varies from ϕ_{min} = 5 mm to ϕ_{max} = 12.5 mm. The cement matrix and the ITZ are assumed to have an analogous diffusivity coefficient. No flux exchange is on the lateral and top surfaces
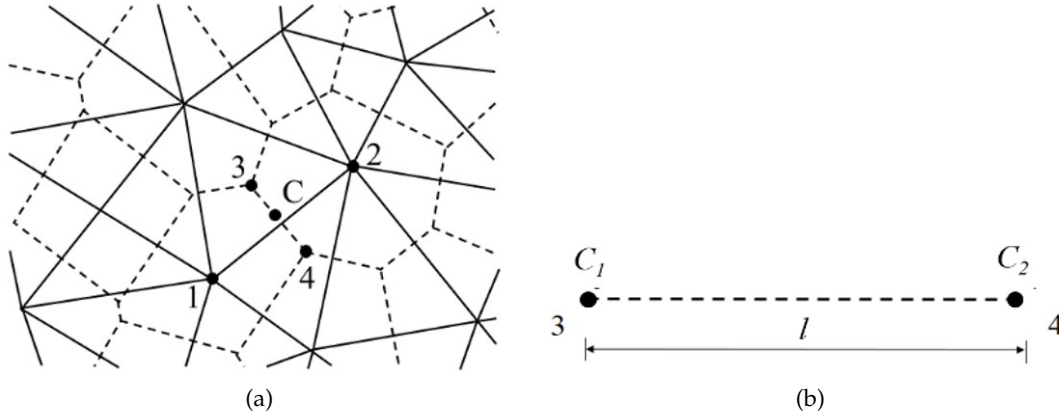
Fig. 1. Structure of the lattices: (a) dual Delaunay triangles and Voronoi polygons for thermo-mechanical or hydro-mechanical coupling; (b) conduit element
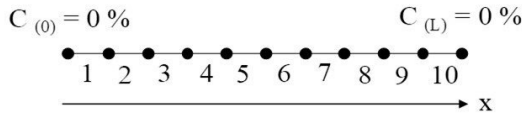
Fig. 2. 1D Chloride ions diffusion
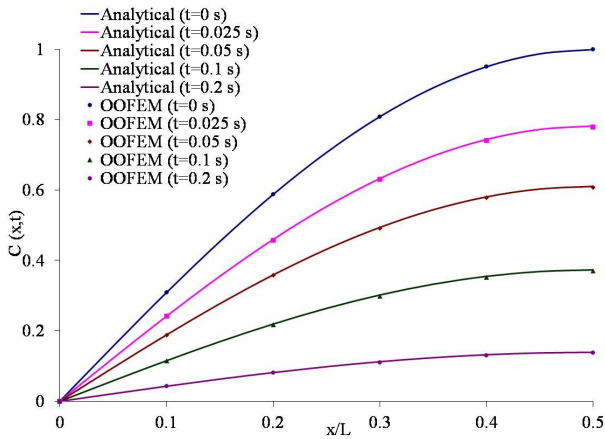
Fig. 3. Comparison between the present model and the closed-form solution (5)

of the sample, while the concentration $C_s(t)$ is prescribed on its bottom surface. The function C_s is taken from the long term measurement of the costal condition of Da Nang City in Vietnam.

2.4. Model Parameters

The input data of the mesoscale lattice model is the properties of concrete constitution: aggregate, cement matrix, ITZ, as well as their volume fraction. Whereas, the measure only gives the macroscopic diffusivity of concrete. This section is dedicated to determine the diffusivity coefficient of

Table 1. Mix-designs for the concrete G40

Material ID	G40
W/C	0.36
Cement PCB40 [kg/m^3]	453
Sand (0-2.5 mm) [kg/m^3]	635
Gravel (2.5-10 mm) [kg/m^3]	1078
Superplasticizer (Glinium) [l/m^3]	4.5
Water [kg/m^3]	165

cement paste D_c and aggregate D_a from the measurement on the sample.

Concrete of grade G40 is considered. The concrete mix-design proportion is shown in Table 1. The size distribution of the aggregate and the sand is displayed in Fig. 5. A super plasticizer Glinium was added. For curing, samples were unmoulded after 24 hours and cured for 28 days in a fog chamber at 100% relative humidity (h_r).

According to ASTM C1202 method (ASTM C1202, 2012), the measurement of the diffusivity coefficient D of the chloride ions is conducted on three cylindrical sample of dimension (100 x 50 mm2). D is determined from the ion permeability Q by using the empirical formulation of [29] as follows:

$$D = 1.03 \times 10^{-14} \times (Q)^{0.84} \qquad (6)$$

The aggregate volume fraction of the concrete G40 f≈0.4. The effect of fly ash is also considered by adding 15% cement mass. Each fly ash exhibits an optimal content depending on its chemical composition. 15% is the optimal content of the considered fly ash. Effect of the fly ash content on the durability of concrete needs further experimental and numerical investigation. Table 2 shows the measured results of the chloride permeability *Q* and the diffusivity coefficient *D* for the concrete without (G40) and
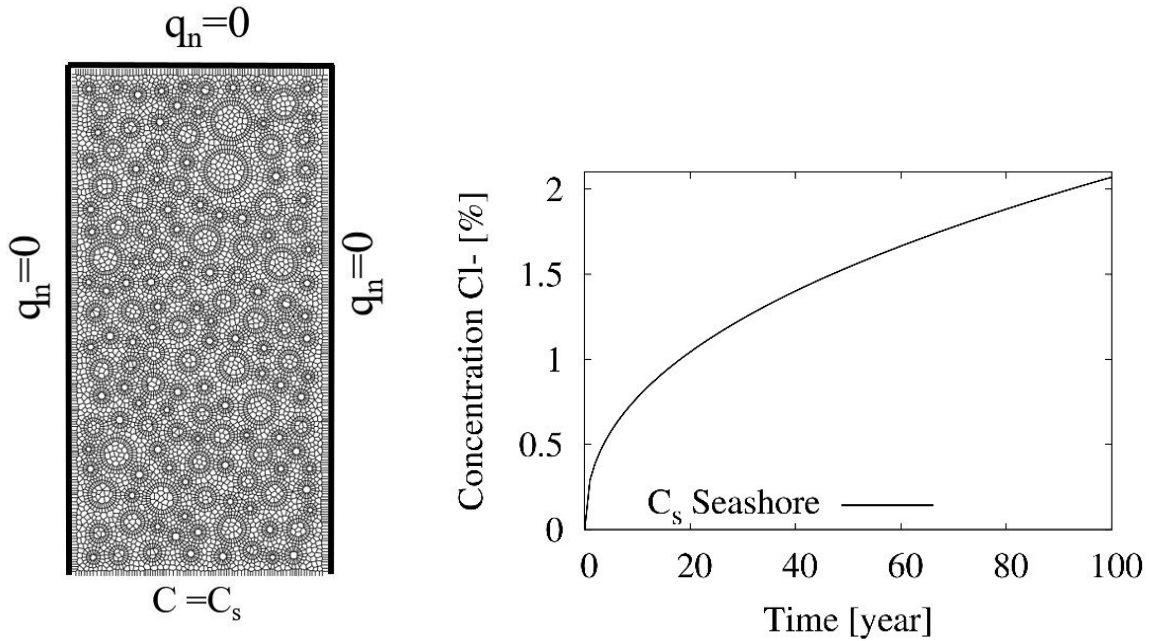
Fig. 4. Geometry and boundary condition of considered numerical model
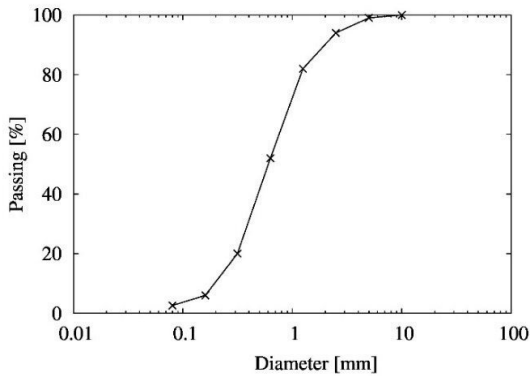
Fig. 5. Granulometric curve of the concrete G40

with fly ash (G40-FA15). The value of D in Table 2 for each concrete type (without or with fly ash) is the average values measured on three samples. However, the variability in the measurement is negligible.

Table 2. Testing chloride ion diffusion in concrete without and with fly ash

Material ID	Q[Coulombs]	D[m^2/s]
G40	2180	656x10^{-14}
G40-FA15	1006	302x10^{-14}

Le [30] considered the concrete as a material of two phases (cement with diffusion coefficient Dc and aggregate with diffusion coefficient Da) and estimated the homoge-

nized diffusivity by using Mori-Tanaka scheme Mori and Tanaka [31] and Hashin and Shtrikman [32] bound (see Fig. 5). Based on her result shown in Fig. 6, D_c = 150.88x10^{-14} (m^2/s) and $D_c/D_a = 10^3$ were assigned to the proposed model for the concrete without fly ash. Introducing these parameters into the lattice model, described in the previous section to compute the variation of the macroscopic diffusion coefficient D as a function of the aggregate volume fraction f. The variation of D as a function of cement volume fraction, 1-f, computed from the present model, is also plotted in Fig. 6. It is worth noting that the maximal aggregate volume fraction is about of 0.7. As observed, the lattice model result is between Mori-Tanaka and Hashin and Shtrikman models. Table 3 recapitulates the diffusivity coefficients of cement paste without and with fly ash, aggregate, and the overall diffusivity of concretes with and without fly ash obtained by the proposed model.

Table 3. Input data and the diffusivity coefficients of G40 and G40-FA15 computed by the lattice model

Concrete/Phases	D[m^2/s]
Aggregate	150.88x10^{-17}
Cement paste without fly ash	150.88x10^{-14}
Cement paste with fly ash	69.63x10^{-14}
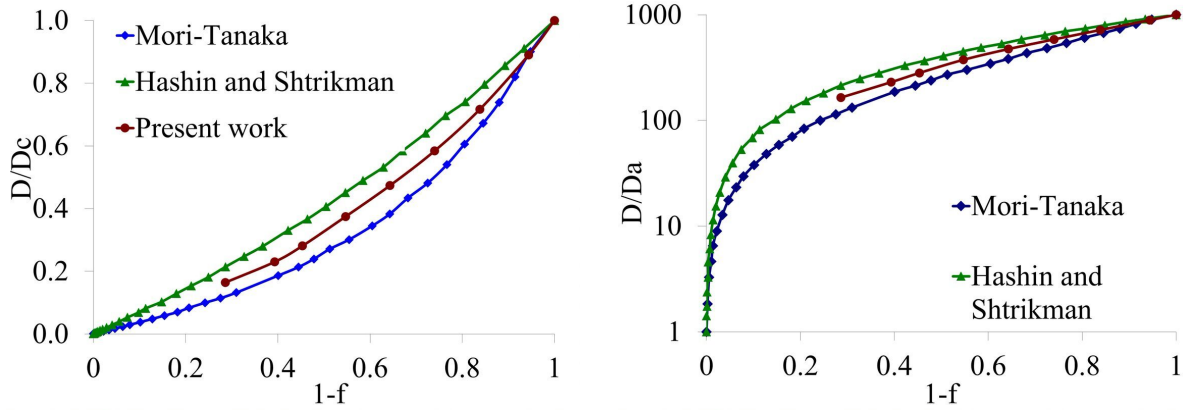
Fig. 6. Diffusivity coefficient of concrete (*D*) versus aggregate volume fraction (1-*f*)

3. Effect of Aggregate Volume Fraction and of Fly Ash

This section is devoted to analyse the effect of volume fraction and of fly ash on the diffusion behavior of concrete. As a reminder, the aggregate volume fraction *f* of the ordinary concrete G40 considered in this study is about 40%. Effects of an increase 10% and of a decrease 10% in the aggregate volume fraction with respect to the concrete G40 on the chloride diffusion coefficient are quantified in this study by mean of the mesoscopic lattice model. Therefore, three values *f* = 30%, 40% and 50% are considered. The lattice samples (F30, F40 and F50) corresponding to these three aggregate volume fractions are shown in Fig. 7.

The boundary condition and the model parameters are described in the previous section. The repartition of the chloride concentration within the sample F40 for different time is shown in Fig 8. The chloride ion rise is not uniform due to the distribution of aggregates.

Fig. **??** plots the evolution of chloride concentration in the four concrete samples: F30 (*f* = 30%), F40 (*f* = 40%), F50 (*f* = 50%), F40FA15 (*f* = 40% with 15% replacement of cement with fly ash) at different distances from the bottom surface where prescribing the function C$_s$(t) shown in Fig. 4. The comparison of chloride diffusion within these four concrete samples is presented in Figure 10. As expected, the sample with a larger aggregate volume fraction resists more the chloride ingress. Indeed, the diffusivity coefficients of F30, F40, F50 are 881x10^{-14} m^2/s; 656x10^{-14} m^2/s; 522x10^{-14} m^2/s, respectively, which is resulted from Fig. 6. Hence, when the diffusivity coefficient of cement paste is kept constant, increase and decrease of 10% of aggregate volume fraction of concrete G40 leads to 25.5% of increasing and decreasing in the overall diffusivity property. Fly ash shows a great benefit about the resistance of

chloride ingress. Table 3 shows that the addition of 15% fly ash content in the cement paste reduces 53.8% the diffusivity coefficient for cement paste and concrete. At the half-height of the sample (i.e. 10 cm), the fly ash reduces 50% of chloride ion migration after 100 years.

4. Cover Thickness-life Service Relation

The cover thickness, corresponding to the chloride concentration threshold C$_{cr}$ defining the service life of structure due to the corrosion, can be determined from the chloride diffusion. These results were described in the previous section (Fig. 9 - 10). According to the recommendation for durability design of concrete structure of DuraCrete DuraCrete [33], the critical chlorite concentration C$_{cr}$ = 0.157%, beyond this value the corrosion of the reinforced steel occurs. Based on Fig. 9 and 10, a service life is determined at different depths from the surface in contact with the aggressive condition (C$_s$(t)) for four concrete samples F30, F40, F50 and F40FA15. As a result, curves, showing the relationship between the concrete cover thickness and its service life, are obtained.

A closed-form solution of cover thickness versus service life can be determined for different grades of concrete. Assuming that the concrete is homogeneous, the 1D solution of the diffusion equation (1) for the configuration drawn in Fig. 4 is:

$$\frac{C}{C_S} = \left(1 - \mathrm{er}f\left(\frac{x}{2\sqrt{D(t)t}}\right)\right) \qquad (7)$$

where C(x,t) (%) is the concentration at the depth x (*m*) and at the time t (*s*); erf(.) the error function; D(*t*) (m^2/s) is the diffusivity coefficient of concrete at the time *t*; C$_s$(t) the loading described in Fig. 4. The function C$_s$(t) is approximated by
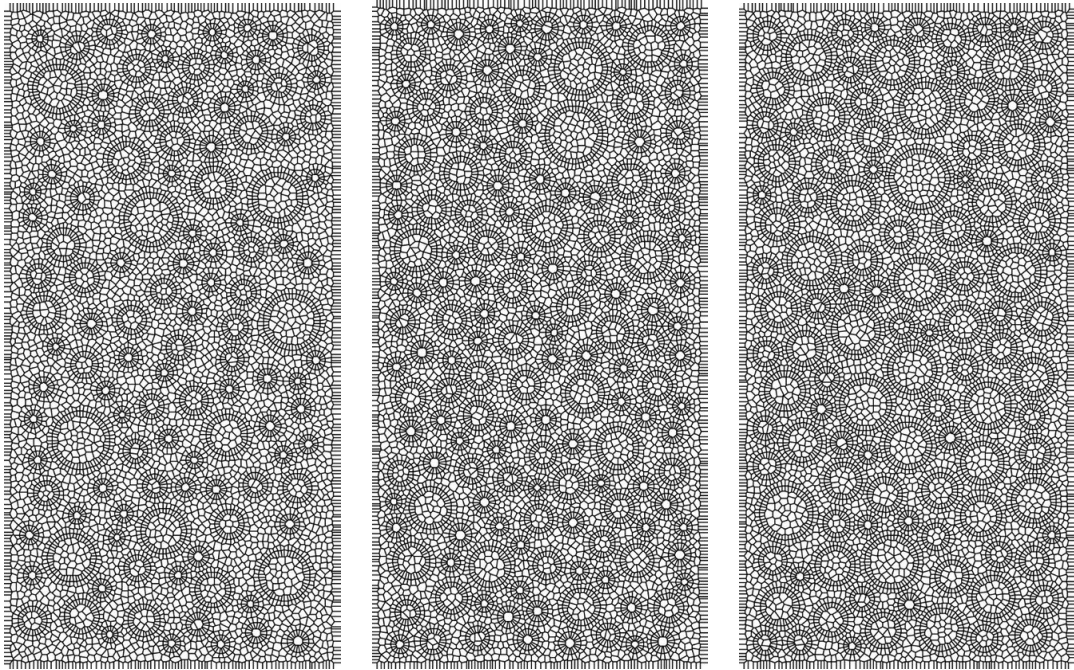
Fig. 7. Concrete samples with the aggregate volume fractions: f = 30% (F30), 40%(F40) and 50%(F50)
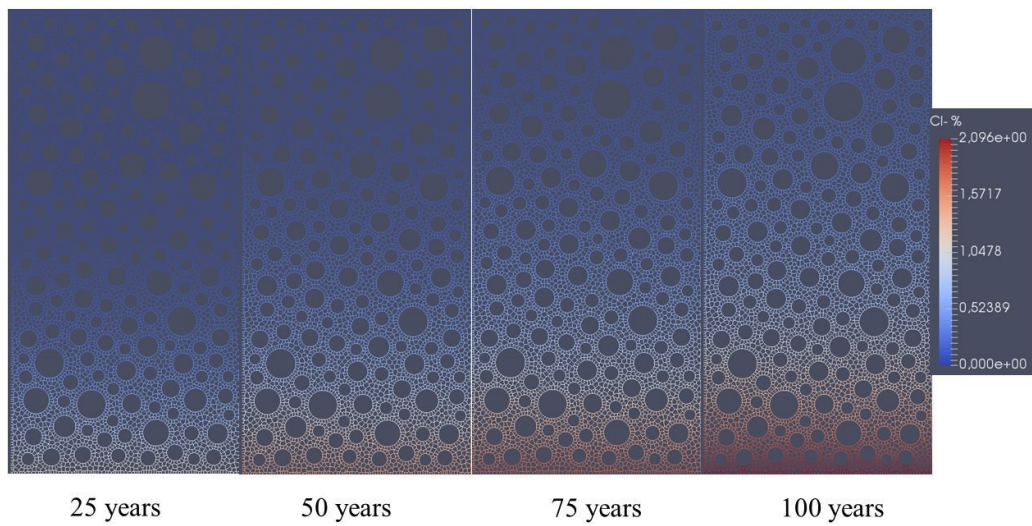
Fig. 8. Chloride distribution within the sample F40
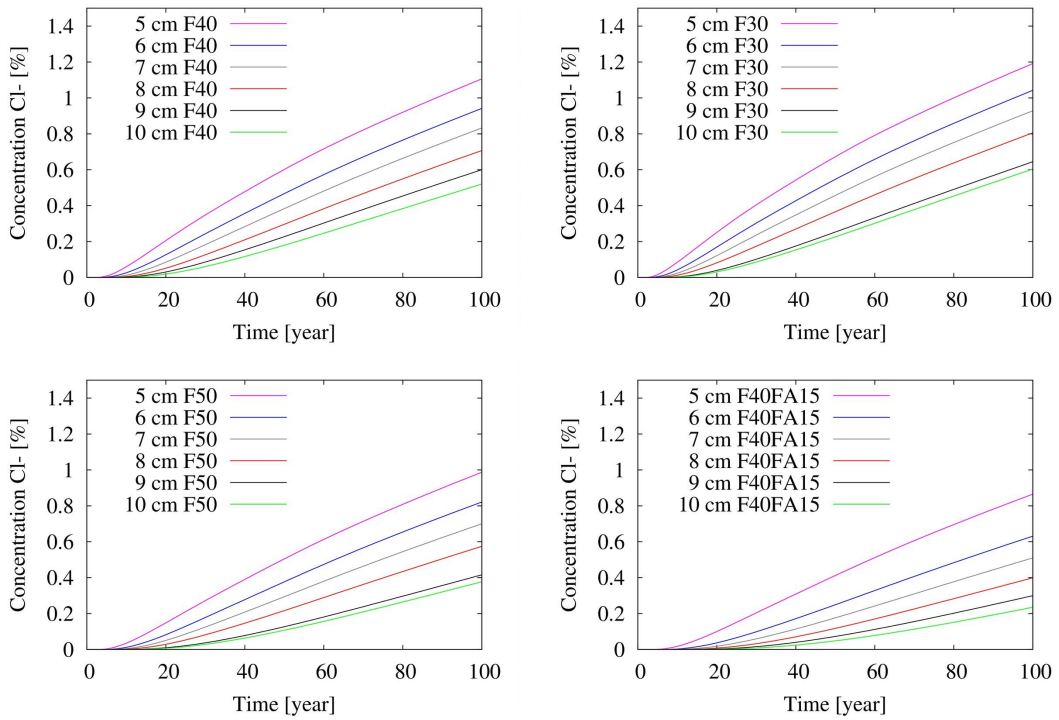
Fig. 9. Evolution of chloride concentration with four concrete samples
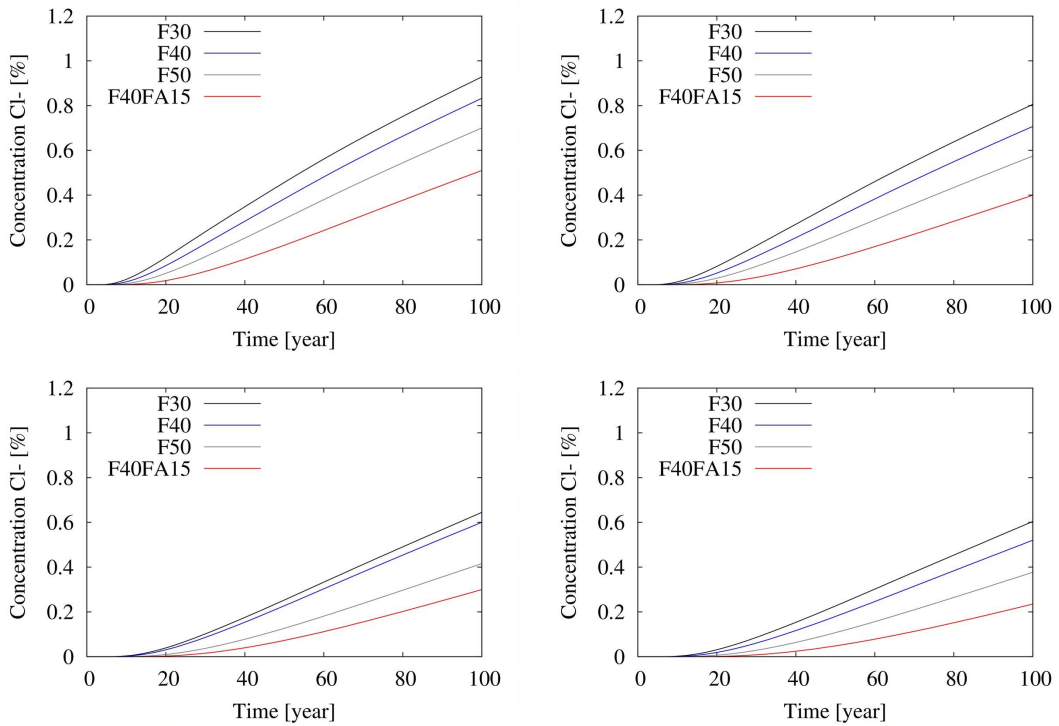
Fig. 10. Effects of aggregate volume fraction and of fly ash on the chloride diffusion in concrete at different position from the surface

$$C_s(t) = \xi t^\lambda \qquad (8)$$

where $\xi = 0.128$ and $\lambda = 0.476$ for coastal condition and $\xi = 0.291$ and $\lambda = 0.426$ for marine condition at Da Nang city.

According to DuraCrete [33] and Life-365 [34]:

$$D(t) = D_0 \left(\frac{t_0}{t} \right)^m \qquad (9)$$

in which D_0 is the diffusivity coefficient at $t_0 = 28$ days; $m = 0.37$; $D_0 = 656 \times 10^{-14}$ (m^2/s) for concrete G40.

Introducing (8) and (9) into (7) yields

$$C(x,t) = \xi t^\lambda \left(1 - \mathrm{er} f \left(\frac{x}{4D_0 t_0^m \cdot t^{1-m}} \right) \right) \qquad (10)$$

Therefore, the cover thickness x corresponding to the service life τ and the chloride concentration threshold C_{cr} is the root of the following equation.

$$C_{cr} = \xi \tau^2 \left(1 - \mathrm{er} f \left(\frac{x}{4D_0 t_0^m \cdot \tau^{1-m}} \right) \right) \qquad (11)$$

As seen in Fig. 11 , a good agreement between the analytical solution and the present model is shown for the concrete G40. A slight difference between them is due to the heterogeneity that is taken into account in the present model. The present closed-form solution (11) for the chloride concentration threshold allows a quick design of the concrete cover thickness corresponding to a durability criterion. This formulation can be also applied for concrete with other grade by changing the parameters D_0 and **m** and/or for other environment condition represented by the function $C_s(t)$.

5. Conclusions

This paper describes a mesoscale lattice model to simulate the chloride diffusion within the concrete structure. Concrete is constituted by three phases: aggregate, cement paste and ITZ, where the diffusion properties of cement matrix and ITZ are assumed to be similar. Chloride diffusion within heterogeneous concrete is represented by Fick's second law. Diffusivity coefficient of cement paste with and without fly ash and that of aggregate are determined by the back analysis from the measurement of the overall diffusivity coefficient of concrete. The effect of aggregate volume fraction and fly ash is considered and evaluated. The following important results can be highlighted.

- The addition of fly ash addition brings about a significant reduction in the chloride ingress in the concrete structure. 15% fly ash content in the cement paste reduces 50% of the chloride concentration at 10 cm of depth from the surface in contact with the aggressive condition in comparison with the concrete G40 without fly ash.

- Increase 10% of aggregate volume fraction reduces 25.5% of the diffusivity coefficient compared to the concrete G40.

- Curves, describing the relation between the concrete cover thickness and the structure service life time, are proposed based on the lattice simulation for concrete G40 with and without fly ash, as well as for three different aggregate volume fractions.

- A closed-form solution is derived for the design of the concrete thickness cover with respect to the concrete grade, the environment concentration of chloride and the chloride concentration criterion induced the rebar corrosion. This analytical solution is in a good agreement with the numerical model for the concrete G40. This solution can be also applied for other concrete grades and for other environment aggressive condition. This finding is meaningful for the design of the RC structure with the consideration of the durability criterion.

The proposed lattice model allows taking into account the heterogeneity and giving the local behaviour of the chloride diffusion. Moreover, this model is applicable for real configuration. The important advantage of the lattice model is the mesh-independent when dealing with the hydro-mechanical coupling in which the mechanical behavior includes the softening strain. Exploitation of this feature is an ongoing work to model the chloride diffusion under stress, which can provoke the damage and failure of concrete structure. Moreover, the influence of the fly ash content on the durability of the concrete is also an upcoming study.

Acknowledgements

References

[1] NTBUILD-443, (1995) *"Concrete Hardened: Accelerated Chloride Penetration"*:

[2] AASHTO. *Standard method of test for resistance of concrete to chloride ion penetration*. 2002.
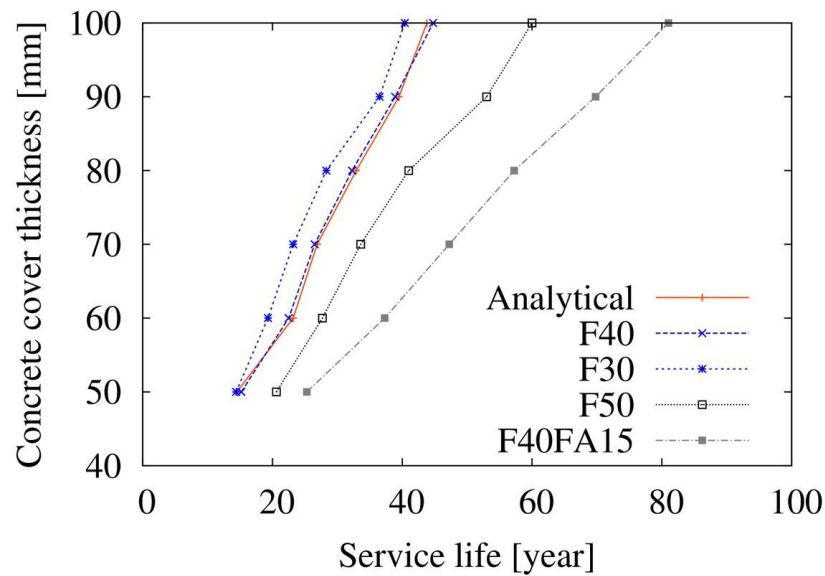
Fig. 11. The relationship between the service life and the concrete cover thickness of the coastal RC structure

[3] G. K. Glass and N. R. Buenfeld, (1998) *"Theoretical assessment of the steady state diffusion cell test"* **Journal of materials science** *33*(21): 5111–5118. DOI: 10.1023/A:1004407214997.

[4] C.-C. Yang and L. C. Wang, (2004) *"The diffusion characteristic of concrete with mineral admixtures between salt ponding test and accelerated chloride migration test"* **Materials Chemistry and Physics** *85*(2-3): 266–272. DOI: 10.1016/j.matchemphys.2003.12.025.

[5] M. Nokken, A. Boddy, R. Hooton, and M. Thomas, (2006) *"Time dependent diffusion in concrete—three laboratory studies"* **Cement and Concrete Research** *36*(1): 200–207. DOI: 10.1016/j.cemconres.2004.03.030.

[6] D. P. Bentz, E. J. Garboczi, and E. S. Lagergren, (1998) *"Multi-scale microstructural modeling of concrete diffusivity: Identification of significant varibles"* **Cement, Concrete and Aggregates** *20*(1): 129–139. DOI: 10.1520/cca10446j.

[7] C.-C. Yang and S.-H. Weng, (2013) *"A three-phase model for predicting the effective chloride migration coefficient of ITZ in cement-based materials"* **Magazine of concrete research** *65*(3): 193–201. DOI: 10.1680/macr.12.00052.

[8] S.-T. Nguyen, D.-C. Pham, M.-N. Vu, and Q.-D. To, (2016) *"On the effective transport properties of heterogeneous materials"* **International Journal of Engineering Science** *104*: 75–86. DOI: 10.1016/J.IJENGSCI.2016.04.001.

[9] A. Pouya, (2015) *"A finite element method for modeling coupled flow and deformation in porous fractured media"* **International Journal for Numerical and Analytical Methods in Geomechanics** *39*(16): 1836–1852. DOI: 10.1002/nag.2384.

[10] M. N. Vu, S. T. Nguyen, and M. H. Vu, (2015) *"Modeling of fluid flow through fractured porous media by a single boundary integral equation"* **Engineering Analysis with Boundary Elements** *59*: 166–171. DOI: 10.1016/j.enganabound.2015.06.003.

[11] M. N. Vu. *Modélisation des écoulements dans des milieux poreux fracturés par la méthode des équations aux intégrales singulières*. 2012.

[12] M. Bitaraf and S. Mohammadi, (2008) *"Analysis of chloride diffusion in concrete structures for prediction of initiation time of corrosion using a new meshless approach"* **Construction and Building Materials** *22*(4): 546–556. DOI: 10.1016/j.conbuildmat.2006.11.005.

[13] A. Daoud, O. Maurel, and C. Laborderie, (2013) *"2D mesoscopic modelling of bar–concrete bond"* **Engineering Structures** *49*: 696–706. DOI: 10.1016/j.engstruct.2012.11.018.

[14] A. Michou, A. Hilaire, F. Benboudjema, G. Nahas, P. Wyniecki, and Y. Berthaud, (2015) *"Reinforcement–concrete bond behavior: Experimentation in drying conditions and meso-scale modeling"* **Engineering Structures** *101*: 570–582. DOI: 10.1016/j.engstruct.2015.07.028.

[15] A. Caggiano and G. Etse, (2015) *"Coupled thermo–mechanical interface model for concrete failure analysis under high temperature"* **Computer Methods in Applied Mechanics and Engineering** *289*: 498–516. DOI: 10.1016/j.cma.2015.02.016.

[16] A. Pouya, M.-N. Vu, S. Ghabezloo, and Z. Bendjeddou, (2013) *"Effective permeability of cracked unsaturated porous materials"* **International Journal of Solids and Structures** *50*(20-21): 3297–3307. DOI: 10.1016/j.ijsolstr.2013.05.027.

[17] J. E. Bolander and N. Sukumar, (2005) *"Irregular lattice model for quasistatic crack propagation"* **Physical Review B** *71*(9): 94106. DOI: 10.1103/PhysRevB.71.094106.

[18] T.-D. Nguyen, D.-T. Pham, and M.-N. Vu, (2019) *"Thermo-mechanically-induced thermal conductivity change and its effect on the behaviour of concrete"* **Construction and Building Materials** *198*: 98–105. DOI: 10.1016/j.conbuildmat.2018.11.146.

[19] D. T. Pham, T. D. Nguyen, M. N. Vu, and A. Chinkulkijniwat, (2019) *"Mesoscale approach to numerical modelling of thermo-mechanical behaviour of concrete at high temperature"* **European Journal of Environmental and Civil Engineering**: 1–20. DOI: 10.1080/19648189.2019.1577762.

[20] D. T. Pham, L. Sorelli, M. Fafard, and M.-N. Vu, (2021) *"Hydromechanical couplings of reinforced tensioned members of steel fiber reinforced concrete by dual lattice model"* **International Journal for Numerical and Analytical Methods in Geomechanics** *45*(2): 191–207. DOI: 10.1002/nag.3148.

[21] P. Grassl, H. S. Wong, and N. R. Buenfeld, (2010) *"Influence of aggregate size and volume fraction on shrinkage induced micro-cracking of concrete and mortar"* **Cement and concrete research** *40*(1): 85–93. DOI: 10.1016/j.cemconres.2009.09.012.

[22] T. Tran, D. Pham, M. Vu, V. Truong, X. Ho, N. Tran, T. Nguyen-Sy, and Q. To, (2021) *"Relation between water permeability and chloride diffusivity of concrete under compressive stress: Experimental investigation and mesoscale lattice modelling"* **Construction and Building Materials** *267*: 121164. DOI: 10.1016/j.conbuildmat.2020.121164.

[23] T. S. Bui, D. T. Pham, M. N. Vu, T. N. Nguyen, T. Nguyen-Sy, V. P. Nguyen, and T. Nguyen-Thoi, (2021) *"Modeling of the tension stiffening behavior and the water permeability change of steel bar reinforcing concrete using mesoscopic and macroscopic hydro-mechanical*

lattice model" **Construction and Building Materials** *291*: 123266. DOI: 10.1016/J.CONBUILDMAT.2021.123266.

[24] P. Grassl and Z. P. Bažant, (2009) *"Random lattice-particle simulation of statistical size effect in quasi-brittle structures failing at crack initiation"* **Journal of engineering mechanics** *135*(2): 85–92.

[25] A. B. Okabe and B. Boots. *B. Sugihara K. and Chiu SN [2000]: Spatial Tessellations: Concepts and Applications of Voronoi Diagrams.* DOI: 10.1002/9780470317013.

[26] J. E. Bolander Jr and S. Berton, (2004) *"Simulation of shrinkage induced cracking in cement composite overlays"* **Cement and Concrete Composites** *26*(7): 861–871. DOI: 10.1016/j.cemconcomp.2003.04.001.

[27] L. Shen, Q. Ren, N. Xia, L. Sun, and X. Xia, (2015) *"Mesoscopic numerical simulation of effective thermal conductivity of tensile cracked concrete"* **Construction and Building Materials** *95*: 467–475. DOI: 10.1016/j.conbuildmat.2015.07.117.

[28] J. Skrzypek and A. Ganczarski. *Modeling of material damage and failure of structures: theory and applications.* Springer Science Business Media, 1999. DOI: 10.1007/978-3-540-69637-7.

[29] N. S. Berke and M. C. Hicks. "Estimating the life cycle of reinforced concrete decks and marine piles using laboratory diffusion and corrosion data". In: *Corrosion forms and control for infrastructure.* ASTM International, 1992. DOI: 10.1520/STP19764S.

[30] T. T. H. Le. *Étude multi-échelle du comportement thermo-hydro-mécanique des matériaux cimentaires: approche morphologique pour la prise en compte de la mésostructure.* 2011.

[31] T. Mori and K. Tanaka, (1973) *"Average stress in matrix and average elastic energy of materials with misfitting inclusions"* **Acta metallurgica** *21*(5): 571–574. DOI: 10.1016/0001-6160(73)90064-3.

[32] Z. Hashin and S. Shtrikman, (1962) *"A variational approach to the theory of the elastic behaviour of polycrystals"* **Journal of the Mechanics and Physics of Solids** *10*(4): 343–352. DOI: 10.1016/0022-5096(62)90005-4.

[33] DuraCrete, (2000) *"Final technical report-general guidelines for durability design and redesign"*:

[34] Life-365, (2013) *"Service Life Prediction model and computer Program for Predicting the Service Life and Life-Cycle Cost of Reinforced Concrete Exposed to Chlorides. Version 2.2"*: